arXiv:astro-ph/0409742v1 30 Sep 2004

The Aquarius Superclusters II. Spectroscopic and Photometric Data[1]

César A. Caretta[2,3], Marcio A. G. Maia[4,2], Christopher N. A. Willmer[5,2]
caretta@lac.inpe.br, maia@ov.ufrj.br, cnaw@ucolick.org

ABSTRACT

We present spectroscopic and photometric data for 920 galaxies selected in 68 fields of the Aquarius Cluster Catalog. Typically the 15 brightest candidate members with magnitudes in the range $16 < b_J < 21$ were selected for observations, and $\sim 71\%$ turn out to be cluster members. Using the new redshift determinations we assign galaxies to groups and clusters, and by including data from the literature we calculate systemic velocities and velocity dispersions for 74 clusters, each with redshifts measured for at least 6 individual galaxies.

Subject headings: galaxies: redshifts — galaxies: clusters: general — galaxies: clusters: superclusters — surveys

1. Introduction

Because of the large number of galaxies contained by superclusters, before the era of large-scale multi-object surveys like 2dFGRS (Colless et al. 2001) and SDSS (Strauss et al. 2002) much of what is known of the properties of these structures has relied mainly on pointed observations, where only a sub-sample of supercluster members is observed spectroscopically. Examples of superclusters that have been studied using this strategy are Pisces-Perseus (e.g., Wegner, Haynes & Giovanelli 1993), Hydra-Centaurus (e.g., da Costa et al. 1986, 1987), Coma-A1367 (e.g., Gregory & Thompson 1978), Hercules (e.g., Barmby & Huchra 1998), Shapley (e.g., Quintana, Carrasco & Reisenegger 2000) and Corona Borealis (e.g., Postman, Geller & Huchra 1988).

In Caretta et al. (2002), hereafter Paper I, we presented a list of candidates clusters and groups in the Aquarius region, comprising the area of sky limited by $22^h57.^m0 < \alpha_{2000} < 23^h38.^m6$, and $-25°54' < \delta_{2000} < -19°29'$. Of the 102 candidates, 39 were new detections. We also presented mean redshifts for 31 previously unobserved clusters and improved redshifts for a further 35. About half of the observed candidates are single concentrations of galaxies, while the remainder are superposition of two or more poor clusters or groups along the line of sight. Using a percolation analysis on the data we found two superclusters of galaxies in Aquarius, one located at $z \sim 0.086$, and another at $z \sim 0.112$. These results differ from Batuski et al. (1999) who claimed finding a single structure of ~ 110 h^{-1} Mpc oriented along the line of sight. More recent work by Smith et al. (2004), aimed at measuring the redshift distribution of weak lensing sources, probed a part of this region of sky using the Two Degree Field system. They detect 48 clusters in the region, of which 22

[1]Partly based on observations at European Southern Observatory (ESO) at the ESO Schmidt, and the 1.52m telescope under the ESO-ON agreement; Observatório do Pico dos Dias, operated by the Laboratório Nacional de Astrofísica (LNA); and Complejo Astronomico El Leoncito (CASLEO), operated under agreement between the Consejo Nacional de Investigaciones Científicas de la República Argentina and the National Universities of La Plata, Córdoba and San Juan.

[2]Observatório Nacional (ON/MCT), Rua Gal. José Cristino, 77 – 20921-400, Rio de Janeiro (RJ), Brazil.

[3]Depto. de Educação, Museu de Astronomia e Ciências Afins (MAst/MCT), Rua Gal. Bruce, 586 – 20921-030, Rio de Janeiro (RJ), Brazil.

[4]Depto. de Astronomia, Observatório do Valongo (OV/UFRJ), Ladeira Pedro Antônio, 43 – 20080-090, Rio de Janeiro (RJ), Brazil.

[5]UCO/Lick Observatory, University of California, Santa Cruz, CA 95064, USA.

are in common with paper I sources.

In this paper we present the spectroscopic and photometric data of our survey. In section 2 we describe the photometric catalogs, the target selection and the spectroscopic procedure, from observations to redshift estimation. The spectroscopic and photometric data for the galaxies are described in section 3, while the catalog of mean radial velocities and velocity dispersions for the clusters is presented in section 4.

2. The Data

2.1. Photometric Catalog

The selection of galaxies for spectroscopic observations is derived from two sources: the COSMOS/UKST Southern Sky Catalog (SSC, Yentis et al. 1992), for astronomical coordinates, b_J magnitudes and other photometric and shape parameters; and a catalog created from the digitization using the APM machine of R band films obtained with 1.0m Schmidt telescope of ESO (see also Paper I). The catalog of spectroscopic candidates was limited to $b_J \leq 20.2$, where the completeness is about 85% (Caretta, Maia & Willmer 2000). This magnitude limit is roughly the faintest that can be attained within reasonable integration times with 2 m class telescopes, and is faint enough that the luminosity function is probed to $\sim M^*_{b_J}$ at $z \sim 0.2$. More than 90% of the galaxies in the SSC have counterparts in the R catalog (20,687 galaxies), and we estimate that the final completeness of our photometric catalog is above 75% at $b_J = 20.2$. The b_J and R magnitudes are both uncertain to 0.2 mag, while the SSC positions used in this work are accurate to better than 1 arcsec.

2.2. Target selection

Since our goal was to detect the presence of superclusters of galaxies in Aquarius, the observational strategy was designed to select preferentially targets with a greater likelihood of being members of clusters or groups belonging to the superclusters. This was done by identifying significant overdensities in the projected distribution of galaxies. In the later runs, once the R-band data became available, an additional selection criterion was used, which took into account the proportion of red galaxies, under the assumption that most of these would be early-types. This means that our redshift catalog has not sampled the region uniformly and is biased towards red galaxies.

As described in Paper I, the galaxies were selected from a catalog of 102 potential clusters or groups of galaxies. For 68 of these, we selected galaxies located in square fields of $10'$ centered on the surface density peaks within the Abell radius. These typically contained all galaxies in the clusters core, with additional objects that could be part of lower density regions of the supercluster.

A total of 94 square fields were observed, and in cases where previous measurements existed in the literature, our observations would supplement the existing redshifts so that at least 10 galaxies would be available to provide a robust velocity dispersion estimate. The average surface density of galaxies for the entire Aquarius region is ~ 0.1 gal arcmin^{-2} to $b_J = 20.2$; the mean surface density of the fields selected for observations ranged from 0.13 to 0.58 gal arcmin^{-2}. The galaxies selected for observations span from $b_J = 16.0$ to 21.0, usually among the 15 brightest galaxies in the field. Obvious foreground galaxies were excluded, so that typically 10 galaxies were observed per $10' \times 10'$ field, which implies in a sampling rate of $\sim 34\%$.

Whenever possible, the slit was rotated so that two or more galaxies were observed simultaneously. As a result of this strategy, there are 27 additional serendipitous galaxies fainter than $b_J = 20.2$ in our catalog.

2.3. Observational Procedure

We carried out 25 observing runs between 1994 and 2000, using three telescopes: the 1.52m of La Silla Observatory (ESO, Chile); the 1.60m of Observatório do Pico dos Dias (OPD/LNA, Brazil) and the 2.15m of Complejo Astronomico El Leoncito (CASLEO, Argentina). In both 1.52m and 1.60m telescopes we used Boller & Chivens spectrographs, while the 2.15m telescope had a REOSC spectrograph. All spectrographs were mounted at the Cassegrain focus. The log of the observing runs is shown in Table 1, which also presents the instrumental configuration. In Table 2 we present the details about the detector characteristics for the three used instrumental set ups.

For all observations, we covered the wavelength range ($\sim$ 4000-7700 Å), using 300 l/mm diffraction

gratings for 1k pixels CCDs and 600 l/mm gratings for the 2k detectors. This range was chosen in order to enclose most of the main absorption and emission optical lines for galaxies from $z = 0.0$ to 0.2. It contains, in absorption, the CaII K and H lines, the G band, Hβ, MgI, Ca+Fe and NaI D band. The emission lines include [OII], Hβ, [OIII] (at 4958.9 and 5006.8 Å), [OI], [NII] (6548.1 and 6583.6 Å), Hα and [SII] (6716.4 and 6730.8 Å).

Integration times ranged from 20 to 120 min, depending on the magnitude and surface brightness of the objects. Longer exposures were divided in multiples of 20 min for an efficient removal of cosmic rays events. Line comparison lamps (He-Ar, He-Ar+Ne, He-Ar+Fe or Fe-Ar) were obtained immediately before or after each exposure. Sequences of bias, domeflats and dark exposures were obtained every night, and also some twilight sky flat-fields for each run. Observations were done typically in dark and grey time.

2.4. Data Reduction

The data reduction followed a standard procedure using IRAF[1]. This involved removal of bias; subtraction of dark current (only necessary in the first few observing runs); division by flat-field and, in a few rare cases, correcting for illumination using twilight flats; removal of cosmic rays; extraction of the 1-D spectrum; and sky-subtraction. In the process of wavelength calibration and linearization, we used arc lamp spectra extracted using the same apertures as the object frames. The wavelength solutions used seventh- or eighth-order legendre polynomials and the final fits typically used more than 40 lines with rms 0.4Å, 0.15Å and 0.09Å, respectively for CASLEO, OPD and ESO. In the cases of galaxies for which multiple exposures were taken, these were co-added after linearizing.

2.5. Redshift Determination

Redshifts were measured using the cross-correlation (Tonry & Davis 1979) and emission lines analyses, both available in the RVSAO package (Kurtz & Mink 1998). In the cross-correlation we used a set of 15 high-signal to noise template spectra, most derived from spectra in the Southern Sky Redshift Survey (SSRS, da Costa et al. 1998) database. The position, height and width of the highest peak for each template was obtained by fitting a parabola. The significance value of this peak is estimated comparing its height relative to typical noise peaks, and is measured by the "R" parameter. In general, most of the templates give estimates within a velocity interval of about 200 km s^{-1}, and for the final cross-correlation velocity we took the one with the highest signal "R" value.

Whenever emission-lines are present, they are fit by Gaussians, and a final emission velocity is obtained by weighting the redshift measured for each individual line by its error. Some spectra have both cross-correlation and emission-line redshifts. In these cases, for a difference between absorption and emission velocities less than 500 km/s, we considered a combined velocity (mean weighted by the respective errors). The average absorption-emission difference was +48 km s^{-1}, with a rms of 170 km s^{-1}, as shown in Figure 1.

The RVSAO package also estimates internal uncertainties (δv) for the redshift measurements. In the case of cross-correlation redshifts, these are related to the "R" parameter, while for emission-line redshifts, the error is estimated by a combination of the line centering error with the dispersion between the measurements of the different lines. For galaxies with both cross-correlation and emission-line redshifts the final internal errors are calculated in quadrature. The distribution, average and median values of these errors and of the "R" parameter are shown in Figures 2 and 3.

All spectra were visually inpected in order to validate the redshift and also to assign a redshift quality. The criteria for defining these quality flags are summarized below:

- [A] excellent, absorption and/or emission lines are well defined and the "R" parameter (signal-to-noise ratio of the correlation peak) much greater than 3;
- [B] good, absorption and/or emission lines confirmed by visual inspection or similar radial velocities for most of the templates but small "R" (between 2 and 4);
- [C] marginal, "R" greater than 2, but with features either in absorption and/or emission too weak to be firmely confirmed;

[1]The Image Reduction and Analysis Facility (IRAF) is distributed by the National Optical Astronomy Observatories.

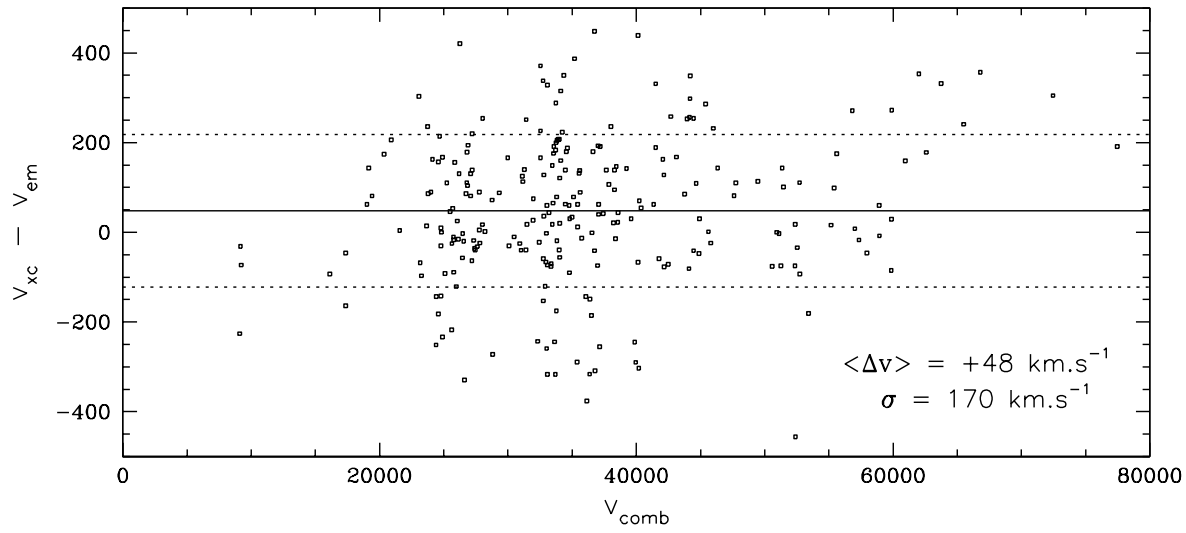

Fig. 1.— Residuals of cross-correlation minus emission-lines velocities as a function of combined velocity. Solid line represents the mean residual value, while dashed lines represent the dispersion.

- [D] failed redshift, "R" < 3 without any identifiable spectral feature.

The fractions of spectra in each of these classes are 74%, 15%, 3% and 8%, respectively for A, B, C and D. In all subsequent analyses only galaxies with redshift qualities of "C" or better will be considered. Typical examples for each of these redshift qualities are shown in Figure 4, for spectra with only absorption-lines; Figure 5, for galaxies with emission lines only; and Figure 6, for galaxies with both emission and absorption. Figure 7a shows the cz-magnitude diagram where solid circles represent galaxies with cross-correlation velocities only, open triangles galaxies with emission-line velocities only and open squares galaxies with both. The distribution of galaxy velocities in Aquarius clearly shows two concentrations, one at c$z \sim$ 26,000 and another at c$z \sim$ 33,500, corresponding to the superclusters described in Paper I. The bottom panel of Figure 7 shows the distribution of redshift quality as a function of magnitude. It is clear that as fainter magnitudes are being probed the number of quality "A" redfshifts (mainly due to cross-correlation) decreases dramatically.

2.6. Redshift Uncertainties

A first check of the reliability of the bulk of our data is done by separating it in sets coming from the three distinct telescopes: C215, O160 and E152 (see tables 1 and 2). Internal velocity errors for all the observed galaxies in each telescope are presented on Table 3, which reveals that ESO data are slightly better (smaller errors), since higher resolution gratings (600 l/mm) were used in this set up. CASLEO data, on the other hand, have slightly higher internal errors, probably due to the noisest CCD used.

Another internal evaluation of redshift uncertainties is done using the radial velocity standard galaxies, observed at least once in every observing night. These are listed on Table 4. Considering only the runs with more than 4 observations of such objects we could estimate the stability in the velocities measured from each telescope. For ESO we have six runs (with 6 to 12 observations each), that give a mean dispersion of 25 km s^{-1}. For OPD we have also six runs (with 4 to 6 observations each) and 30 km s^{-1}. For CASLEO we have only one object in one run, and 28 km s^{-1}. This shows that all the three instrumental set ups produce similar internal dispersions, of about 25-30

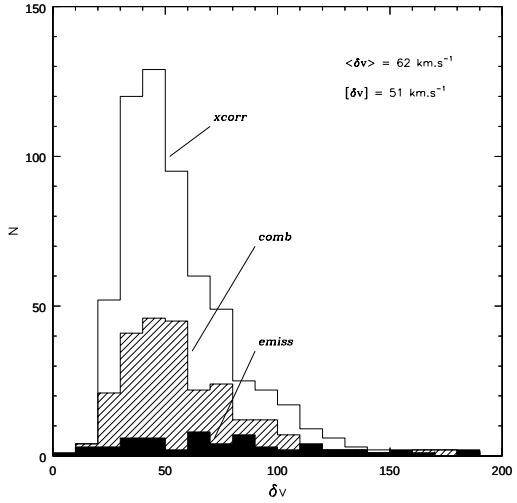

Fig. 2.— Distribution of velocity errors according to the different types of spectra. $< \delta v >$ and $[\delta v]$ refer to, respectively, average and median values for all data.

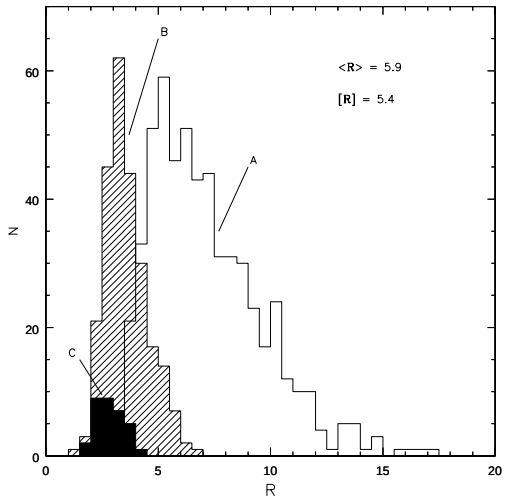

Fig. 3.— Distribution of "R" parameter for quality classes A, B and C. <R> and [R] refer to, respectively, average and median values for all data. Note that the quality class is clearly related to the "R" parameter.

km s^{-1}, for the radial velocity standards. Since they are the best signal to noise data, their dispersion may be considered as a lower limit for our internal uncertainties.

We also used the standard galaxy measured velocities for external comparison, in order to estimate possible zero points between the instrumental set ups used. Column 6 of Table 4 lists the mean velocity differences between ESO and NED velocities, which give, on mean, +15±38 km s^{-1} (for 6 galaxies). Similarly, column 11 show these differences between OPD and NED velocities (also for 6 galaxies), +45±70 km s^{-1} on mean, and column 16 for CASLEO and NED (for only one galaxy), −31 km s^{-1}. The same results are found using mean NED velocities (column 23). Nevertheless, it may be noted that NED velocities are not necessarily the best ones for comparison since they come from different sources (Δv is not systematic for a single instrumental set up).

A further estimate of the redshift uncertainties can be made using galaxies that have more than one measurement carried out by ourselves, as well as comparing our measurements with those available in the literature. For a total of 20 galaxies we obtained spectra in different observing runs. From these measurements, shown in Figure 8a, we find a dispersion of 191 km s^{-1}. Since the number of objects is very small, the dispersion may be overestimated. In Figure 8b we show the comparison for 118 galaxies of our database with redshifts also available on the literature. In this case, we find a zero-point shift of +81 km s^{-1} and standard deviation of 181 km s^{-1}. Most of these galaxies were observed as part of the 2dFGRS (Colless et al. 2001), represented by the symbols other than crosses. When the 97 2dFGRS galaxies are considered the mean difference is +91±156 km s^{-1}. The best estimation of spread in 2dFGRS itself, as measured by the authors, comes from their comparison with Las Campanas Redshift Survey (LCRS, Shectman et al. 1996) data, with gives 109 km s^{-1}. Considering equally distributed errors for the two sources, the 2dFGRS error may be about 77 km s^{-1}. By subtracting quadratically this error to the above measured dispersion, this gives an estimation of the overall error of our data of 136 km s^{-1}. If we now separate the data by instrumental set up (indicated by the different symbols in Figure 8), we find a mean difference of +93±226 km s^{-1} for OPD data (26 galaxies) and +90±123 km s^{-1} for ESO data (70 galaxies). For CASLEO the estimation is not possible due to the small number of

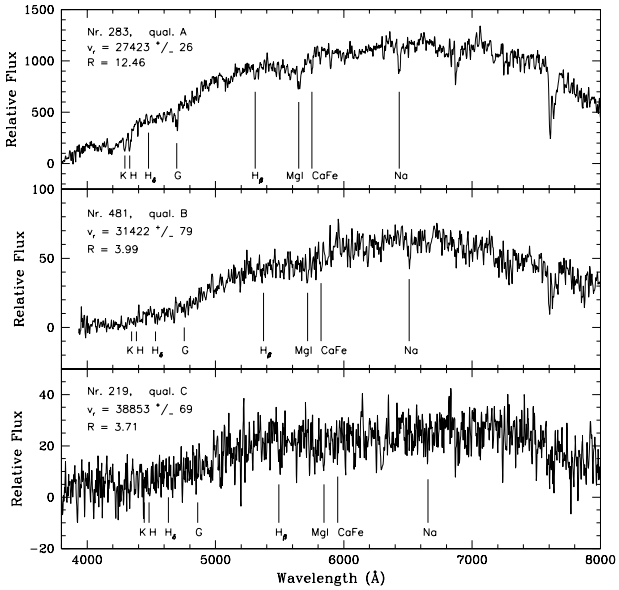

Fig. 4.— Sample of absorption-lines spectra of the three quality classes. Objects are identified by their number in Table 5 (Nr.). Also are displayed their radial velocity (v_r) and "R" parameter of cross-correlation.

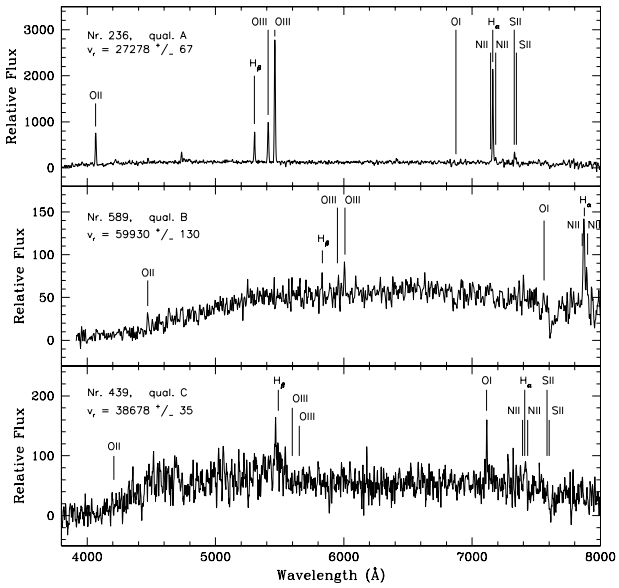

Fig. 5.— Sample of emission-lines spectra of the three quality classes. Identification of objects is the same as in Figure 1.

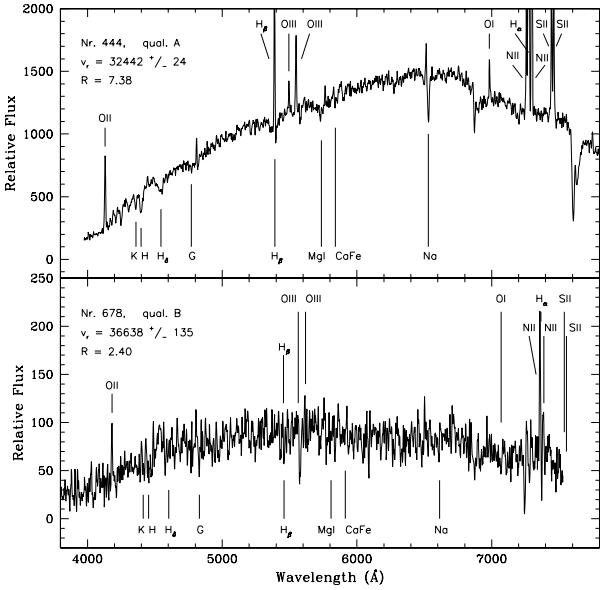

Fig. 6.— Sample of combined absorption and emission spectra, same identifications as in Figure 1.

objects. Thus, both OPD and ESO data have the same zero point related to 2dFGRS data, but the dispersion of OPD data is somewhat higher than ESO data one. Note that the number of galaxies in OPD data is about one third of ESO one, what may be effecting in the large dispersion measured. Since ESO data represent 63% of our overall sample, OPD 34%, and CASLEO only 3%, we can estimate the typical uncertainty in our measured radial velocities by the the weighted mean of ESO and OPD dispersions, 150 km s^{-1}, which is consistent with all the results above.

3. The Aquarius Galaxy Catalog

A total of 920 new galaxy redshifts, with quality grades "C" or better, were measured in the direction of 72 cluster and group candidates, 68 of which within the bounds of the region considered in this work. In addition, we find 2851 redshifts in the literature for the same area of sky, most (2378) coming from the 2dFGRS, but which only contains galaxies located on the southern part of Aquarius region ($\delta < -23.5$).

Our new measurements are listed in Table 5,

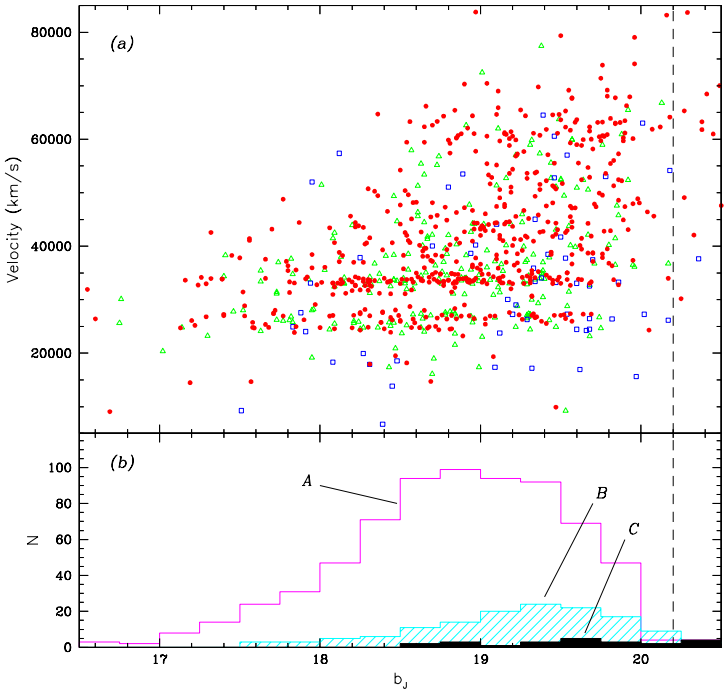

Fig. 7.— (a) Distribution of measured velocities with magnitudes. Solid circles are absorption-line only spectra and open symbols are spectra with emission-lines (triangles for both emission and absorption spectra and squares for only emission ones). Note that absorption line spectra galaxies (probably early-type ones) are slightly more concentrated than the emission line galaxies (probably intermediate and late-type ones). (b) Distribution of quality classes with magnitude. The vertical dashed line represents the b_J=20.2 magnitude limit of the sample.

where we show, in column (1), a sequential number for galaxy identification; in columns (2) and (3), the equatorial coordinates (J2000.0); and b_J and R magnitudes in columns (4) and (5), respectively. When a galaxy is assigned to a group or cluster, column (6) gives the name of the cluster/group; whenever these are assigned to different systems along the same line of sight, suffixes A, B, C are appended to the group name; suffixes 1 and 2 are assigned to the clusters A2538 and A3985, which are only marginally separated in the redshift space. Columns (7) and (8) list the heliocentric velocity and velocity error of the galaxy. The codes on column (9) indicate the type of redshift (x = cross-correlation, e = emission lines, and c = combined cross-correlation and emission lines redshift), the quality grade and the value of the "R" parameter. The observing run, as listed on Table 1, during which the galaxy spectrum was taken, is shown on column (10).

4. Cluster Systemic Velocities and Velocity Dispersions

Combining the data from the Aquarius Galaxy Catalog with the 2851 redshifts from the literature we re-determine the redshifts and velocity dispersions for several of the clusters and groups within the surveyed region. Currently there are 81 candidates of the Aquarius Cluster Catalog with redshifts for galaxies inside their estimated Abell radius, 9 more than published in Paper I. As described in Paper I, about half of the observed candidates show more than one significant peak along the line of sight to the depth of our survey. About 120 peaks were found, ranging from rich clusters to small groups. Here we present radial velocities and velocity dispersions for the systems with at least six measured velocities.

The member galaxies were selected inside a projected circle of 1.5 Mpc radius (H_0 = 75 km s^{-1} Mpc^{-1} hereafter) of the system center. For most of the systems, the center is defined as being coincident with the position of the brightest cluster galaxies (BCG: a cD galaxy, a giant elliptical or a central group of early-type galaxies), since these massive objects tend to be preferentially located close to the bottom of the potential well, as an effect of dynamical friction (Bird 1994). For systems without apparent dominant galaxies, the mean po-

sition of the members was used. Comparing the centers derived from the BCGs with those measured from the overall distribution of galaxies, and with centers measured from X-rays we find that the uncertainty of the centers is estimated to be ~ 0.1 Mpc. This comparison was done for 12 clusters, namely A2521, A2534, A2536, A2540, A2550, A2554, A2555, A2556, A2566, A2577, A2580 and A2606.

In the cases of galaxies with more than one measurement, these were averaged, unless the redshift quality was poor, in which case only the best measurement was used. The redshift extent of the individual groups and clusters was defined using the gaps method (e.g., Zabludoff, Huchra & Geller 1990; Katgert et al. 1996), initially selecting galaxies whose separation from their neighboring members was less than 1500 km s^{-1}. This value was chosen based on the characteristic projected density of the sample. Smaller gaps, weighted by their location with respect to the middle of the cluster velocities distribution, were calculated during a second step of robust estimation of parameters and used iteratively to exclude remaining interlopers.

The final systemic velocity and velocity dispersion were calculated through robust estimation of the biweighted center and scale (Beers, Flynn & Gebhardt 1990). The results for 74 Aquarius clusters are presented in Table 6. Column (1) lists the AqrCC number of the observed candidate, while column (2) shows another identification. Equatorial coordinates of system center are shown in columns (3) and (4). Column (5) indicates if the chosen projected center was the BCG(s) position or the geometric mean of members positions. The number of galaxies identified as members from the Aquarius Galaxy Catalog is shown in column (6), while the number of such redshifts from the literature is in column (7). Column (8) gives the reference for literature redshifts. The total number of member galaxies whose velocities were used to calculate the systemic velocity is in column (9). Note that, since there are repeated observations from both this work and from the literature, the total number of members with redshifts can be smaller than the sum of the numbers from the two sources. Columns (10) and (11) show, respectively, the system velocity and velocity dispersion, both with 68% bootstrap confidence level uncertainty limits.

Comparing the current data with the one on Paper I, for 25 cluster the estimates remained unchanged, other 30 had their systemic velocities upgraded due to inclusion of 2dFGRS velocities or more robust calculations, and 3 new ones were added. Major differences are presented by A2538 and A3985 that were splitted in redshift space and APM895 and APM894 which are now considered a single system. Another improvement was the estimation of velocity dispersions for the clusters. Concerning to the work of Smith et al. (2004), they have 12 clusters in common with Table 6 ones, most of which with a larger number of galaxies observed by they. From these, 11 have similar redshifts to the ones here. The only one with a slightly discrepant value is A2540, for which we have measured galaxies only in the core of the cluster, and their value may be more representative. Comparing the velocity dispersions of the two sources one finds that 11 of the 12 clusters in common have higher values in their estimation. This may also be due to the sampling of larger areas and to a less restrictive criteria for defining cluster members they used. So, two effects may be playing role on this difference: our data underestimate whole system velocity dispersions and/or their data may be overestimated by residual interlopers. The cluster A2554, on the other hand, has higher velocity dispersion in our data by 188 km s^{-1}. Since Smith et al. (2004) used almost two times the number of member galaxies we used, and a larger area, this could indicate that this cluster has a declining velocity dispersion profile on the outskirts (not common but possible). The velocity dispersion profile of A2554 has been calculated by Fadda et al. (1996), and do not show evidence of a declining profile. The overall velocity dispersion calculated by these authors is similar to our value (840^{+131}_{-68} km s^{-1}, for 28 member galaxies).

Finally, one should note that two clusters in our sample, A2540 and A2547, have estimated velocity dispersions much smaller than their uncertainty limits. For such clusters all the observed member galaxies (9 and 15, respectively) have close radial velocities, which low probability of happen gave the high estimated uncertainty limits. Such velocity dispersion must be used with care. If we consider the velocity dispersion differences (excluding A2540 and A2554) between our and Smith et al.

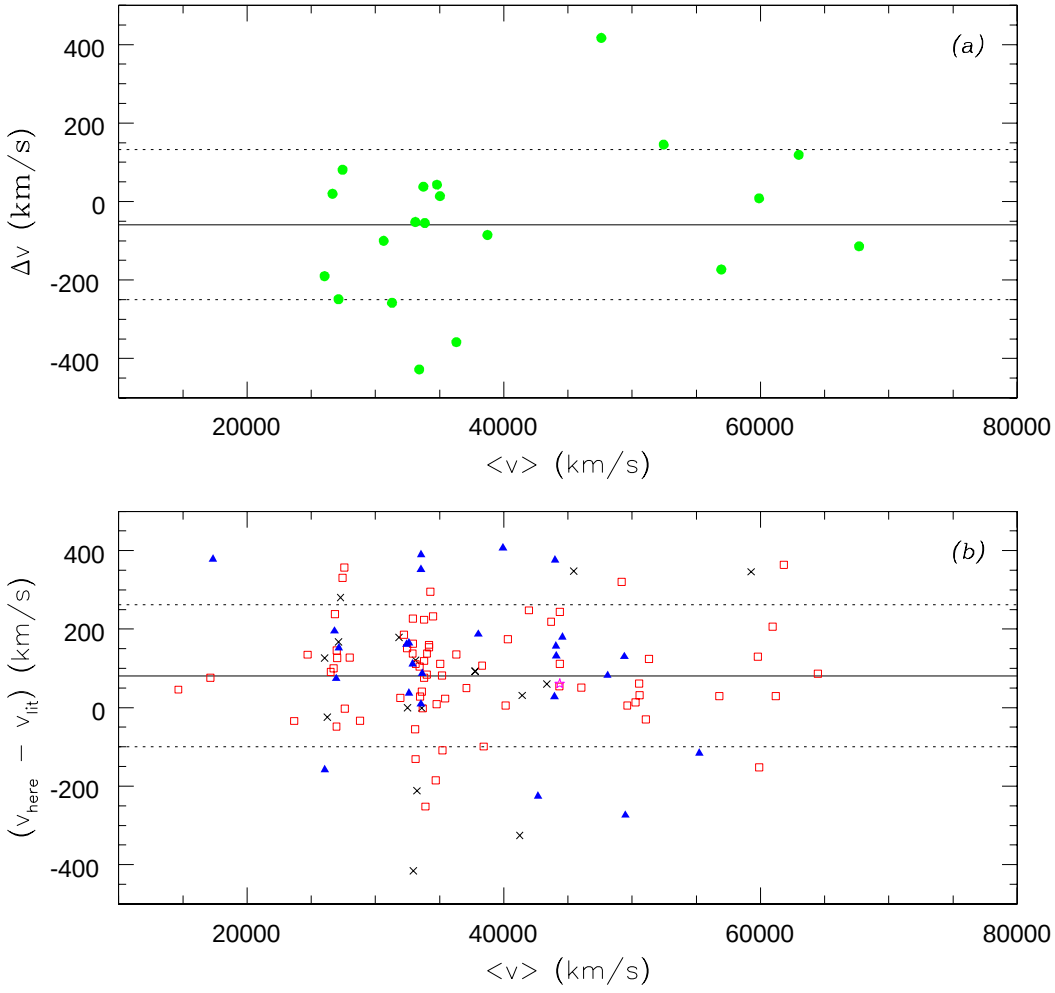

Fig. 8.— (a) Velocity residuals from our repeated observations (solid circles). (b) Velocity residuals between our data and data from the literature, separated in datasets from distinct telescope: open squares = E152 × 2dFGRS; solid triangles = O160 × 2dFGRS; open star = C215 × 2dFGRS; crosses = all telescopes × other sources from the literature.

(2004) data, we find a mean difference of 215 km s^{-1}, that may be considered as the maximum underestimation for the whole cluster velocity dispersions of our measurements restricted to a few more than the cluster cores.

5. Summary

We presented photometry and spectroscopic redshifts for a sample of 920 galaxies in the Aquarius region, most of which selected as candidate members of potential groups and clusters in the region.

We described the target selection and observational procedures as well the redshifts estimation and error analysis. The results are presented in two separated tables, one is the Aquarius Galaxy (radial velocity and photometric) Catalog and the other is the cluster systemic velocity and velocity dispersion list.

The strategy of priorizing red galaxies was successful since 85% of the observed galaxies provided a cross-correlation redshift (92% of the final catalog), and 71% of the galaxies were confirmed as cluster or group members.

The two main superclusters in the region, at $z \sim 0.086$ and $z \sim 0.112$, are clearly seen in the distribution of galaxy redshifts.

From the 81 candidates of AqrCC with observations up to date, we selected 58, that present clusters with at least six members with redshifts (a total of 74 clusters due to superposition along the line of sight), to have their systemic velocities and velocity dispersions calculated. The other 23 observed candidates are 14 with less than six members with redshifts (but indicated by their member galaxies in the Aquarius Galaxy Catalog), 4 that were observed but not confirmed as clusters or groups, and 5 that appear in Smith et al. (2004).

The systemic velocities presented here are updates to the cluster catalog of Paper I, with the addition of cluster velocity dispersions, but essentially the conclusions reached in that paper remain unchanged.

We are grateful to the staff and night assistants of OPD/LNA 1.6m, ESO 1.52m and CASLEO 2.15m; the AAO and NRL/ROE for providing the SSC. We also thank the referee for his helpful suggestions. This research has also made use of NASA/IPAC Extragalactic Database (NED). C.A.C. acknowledges CNPq grant 380577/02-0, M.A.G.M. CNPq grants 301366/86-1, 471022/03-9 and 305529/03-0. C.N.A.W. has been supported by the NSF grants AST 95-29098 and AST 00-71198.

REFERENCES

Alonso, M.V., Valotto, C., Lambas, D.G., & Muriel, H. 1999. MNRAS, 308, 618

Alonso, M.V., Bernardi, M., da Costa, L.N., Wegner, G., Willmer, C.N.A., Pellegrini, P.S. & Maia, M.A.G. 2003. AJ, 125, 2307

Barmby, P., & Huchra, J.P. 1998. AJ, 115, 6

Batuski, D.J., Maurogordato, S., Balkowski, C., & Olowin, R.P. 1995. A&A, 294, 677

Batuski, D.J., Miller, C.J., Slinglend, K.A., Balkowski, C., Maurogordato, S., Cayatte, V., Felenbock, P., & Olowin, R. 1999. ApJ, 520, 491

Beers, T.C., Flynn, K., & Gebhardt, K. 1990. AJ, 100, 32

Bird, C.M. 1994. AJ, 107, 1637

Caretta, C.A., Maia, M.A.G., & Willmer, C.N.A. 2000. AJ, 119, 524

Caretta, C.A., Maia, M.A.G., Kawasaki, W., & Willmer, C.N.A. 2002. AJ, 123, 1200 (Paper I)

Ciardullo, R., Ford, H., & Harms, R. 1985. ApJ, 293, 69

Colless, M., & Hewett, P. 1987. MNRAS, 224, 453

Colless, M., et al. (The Two Degree Field Galaxy Redshift Survey Team) 2001. MNRAS, 328, 1039

Collins, C.A., Guzzo, L., Nichol, R.C., & Lumsden, S.L. 1995. MNRAS, 274, 1071

da Costa, L.N., Pellegrini, P. S., Willmer, C.N.A., Nunes, M. A., Chincarini, G., & Cowan, J. J. 1986. AJ, 91, 6

da Costa, L.N., Willmer, C.N.A., Pellegrini, P.S., & Chincarini, G. 1987. AJ, 93, 1338

da Costa, L.N., Willmer, C.N.A., Pellegrini, P.S.S., Chaves, O.L., Rité, C., Maia, M.A.G., Geller, M.J., Latham, D.W., Kurtz, M.J., Huchra, J.P., Ramella, M., Fairall, A.P., Smith, C., & Lípari, S. 1998. AJ, 116, 1

Dalton, G.B., Efstathiou, G., Maddox, S.J., & Sutherland, W.J. 1994. MNRAS, 269, 151

Fadda, D., Girardi, M., Giuricin, G., Mardirossian, F, & Mezzetti, M. 1996. ApJ, 473, 670

Gregory, S.A., & Thompson, L.A. 1978. ApJ, 222, 784

Kaldare, R., Colless, M., Raychaudhury, S. & Peterson, B.A. 2003. MNRAS, 339, 652

Kapahi, V.K., Athreya, R.M., Breugel, W.V., McCarthy, P.J., & Subrahmanya, C.R. 1998. ApJS, 118, 275

Katgert, P., Mazure, A., Perea, J., den Hartog, R., Moles, M., Le Fèvre, O., Dubath, P., Focardi, P., Rhee, G., Jones, B., Escalera, E., Biviano, A., Gerbal, D., & Giuricin, G. 1996. A&A, 310, 8

Kowalski, M.P., Ulmer, M.P., & Cruddace, R.G. 1983. ApJ, 268, 540

Kurtz, M.J., & Mink, D.J. 1998. PASP, 110, 934

Longhetti, M., Rampazzo, R., Bressan, A., & Chiosi, C. 1998. A&AS, 130, 267

Loveday, J. 1996. MNRAS, 278, 1025

Owen, F.N., Ledlow, M.J., & Keel, W.C. 1995. AJ, 109, 14

Postman, M., Geller, M.J., & Huchra, J.P. 1988. AJ, 95, 267

Quintana, H. & Ramírez, A. 1995. ApJS, 96, 343

Quintana, H., Carrasco, E.R., & Reisenegger, A. 2000. AJ, 120, 511

Ramella, M., Focardi, P., & Geller, M.J. 1996. A&A, 312, 745

Ratcliffe, A., Shanks, T., Parker, Q.A., Broadbent, A., Watson, F.G., Oates, A.P., Collins, C.A., & Fong, R. 1998. MNRAS, 300, 417

Shectman, S.A., Landy, S.D., Oemler, A., Tucker, D.L., Lin, H., Kirshner, R.P., & Schechter, P.L. 1996. ApJ, 470, 172

Schneider, D.P., Gunn, J.E., & Hoessel, J.G. 1983. ApJ, 264, 337

Smith, R.E., Dahle, H., Maddox, S.J., Lilje, P.B. 2004, preprint (astro-ph/0401641)

Strauss, M.A., et al. (The Sloan Digital Sky Survey Team) 2002. AJ, 124, 1810

Tonry, J., & Davis, M. 1979. AJ, 84, 1511

Valentijn, E.A., & Casertano, S. 1988. A&A, 206, 27

Wegner, G., Haynes, M.P., & Giovanelli, R. 1993. AJ, 105, 1251

Yentis, D. J., Cruddace, R. G., Gursky, H., Stuart, B. V., Wallin, J. F., MacGillivray, H. T., & Collins, C. A. 1992. In *Digitised Optical Sky Surveys*, eds. H. T. MacGillivray & E. B. Thomson (Kluwer: Dordrecht), p. 67

Zabludoff, A.I., Huchra, J.P., & Geller, M.J. 1990. ApJS, 74, 1

This 2-column preprint was prepared with the AAS LaTeX macros v5.2.

TABLE 1
OBSERVING RUNS

Run (1)	Telescope* (2)	Date (3)	Grating (l/mm) (4)	Slit (μm) (5)	Detector† # (6)	Disp. (Å/pix) (7)	Resol. (Å) (8)	Range $\lambda\lambda$ (9)	Targets‡ (10)	Objects‡ (11)
1	C215	sep94	316	500	Tek	3.2	18	4760-7980	9	9
2	O160	oct94	300	600	048	4.1	14	4200-8260	9	11
3	O160	aug95	300	450	048	4.1	12	4360-8420	35	39
4	O160	aug96	600/300	500/400	101	4.3	11	3560-8120	18	19
5	C215	sep96	300	400	Tek	3.2	16	4200-7660	35	38
6	E152	nov96	600	419	039	1.9	4	3972-7838	37	42
7	E152	jun97	600	419	039	1.9	4	3800-7700	15	16
8	O160	aug97	300	400	101	4.3	11	3650-8050	13	14
9	E152	aug97	600	419	039	1.9	4	3600-7500	53	117
10	O160	oct97	300	400	101	4.3	11	3700-8100	17	25
11	E152	oct97	600	400	039	1.9	4	3639-7537	12	29
12	E152	jun98	600	400	039	1.9	4	3634-7518	2	6
13	E152	aug98	600	400	039	1.9	4	3640-7520	52	121
14	O160	aug98	300	400	106	4.3	11	3700-8100	23	36
15	E152	oct98	600	400	039	1.9	4	3515-7514	4	9
16	O160	aug99	300	350	106	4.3	10	3700-8100	19	36
17	E152	aug99	600	400	039	1.9	4	3680-7560	2	5
18	O160	sep99	300	350	106	4.3	10	3750-8150	28	46
19	E152	oct99	600	400/350	038	1.9	4	3300-8650	16	33
20	E152	dec99	600	400	038	1.9	4	3400-8500	36	80
21	O160	aug00	300	250	106	4.3	8	3700-8100	36	67
22	E152	sep00	600	400	038	1.9	4	3370-8492	34	68
23	O160	sep00	300	250	106	4.3	8	3700-8100	9	19
24	O160	oct00	300	250	106	4.3	8	3700-8100	6	15
25	E152	nov00	600	250	038	1.9	3	3350-8450	43	93

*Instrumental set up: C215 = CASLEO 2.15m + REOSC; O160 = OPD 1.60m + B&C; and E152 = ESO 1.52m + B&C

†Details on table 2

‡Number of pointed "targets" and final number of observed "objects" with successful redshift measurement (due to multiobjects on the slit).

TABLE 2
CHARACTERISTICS OF THE DETECTORS AND INSTRUMENTAL SET UP USED

CCD Nr. (1)	Origin (2)	Dimensions (pixels) (3)	Pixel (μm) (4)	Gain (e^-/ADU) (5)	Noise (e^- *rms*) (6)	Scale (7)	Efficiency (4000-8000) (8)	Telescope (9)
	Tek	1024×1024	24	2.0	7.4	3.96"/100μm	95-70%	C215
#48	EEV	770×1152	22.5	3.3	6.6	1.04"/100μm	15-45%	O160
#101	SITe	1024×1024	24	5.0	5.5	1.04"/100μm	40-65%	O160
#106	SITe	1024×1024	24	5.0	4.1	1.25"/100μm	55-75%	O160
#39	Loral	2048×2048	15	1.2	5.0	0.82"/100μm	75-95%	E152
#38	Loral	2688×512	15	1.6	7.1	0.82"/100μm	75-90%	E152

Table 3
Average and Median Internal Errors*

Telescope	N	$< \delta v >$	σ_v	$[\delta v]$
E152	581	58	44	48
O160	310	66	39	57
C215	29	87	52	75
all data	920	62	43	51

*<> e [] represent, respectively, mean and median values.

Table 4
Velocity Standard Galaxies*

Galaxy	This work																		NED				
	E152					O160					C215					all data				Small Error †		all data		
(1)	$< v >$ (2)	σ_v (3)	N_r (4)	N_o (5)	Δv (6)	$< v >$ (7)	σ_v (8)	N_r (9)	N_o (10)	Δv (11)	$< v >$ (12)	σ_v (13)	N_r (14)	N_o (15)	Δv (16)	$< v >$ (17)	σ_v (18)	N_o (19)	Δv (20)	v (21)	Ref.§ (22)	$< v >$ (23)	σ_v (24)	N_v (25)
NGC 7507	1594	20	3	12	+28	1616	43	1	3	+50	...	...	...	...	...	1605	25	15	+39	1566±15	1	1577	29	10
NGC 1316	1752	21	2	18	−8	...	...	...	...	...	...	...	...	...	...	1760	11	18	+0	1760±10	2	1795	54	14
NGC 6958	2738	29	7	18	+25	...	...	...	...	...	...	...	...	...	...	2735	30	18	+22	2713±13	1	2687	53	7
NGC 6868	2926	12	4	10	+72	2913	12	1	7	+59	...	...	...	...	...	2917	43	17	+63	2854±15	3	2843	47	8
NGC 5419	...	...	...	...	...	4196	62	3	12	+70	...	...	...	...	...	4173	57	12	+47	4126±15	4	4136	77	7
NGC 6721	4435	13	2	11	+14	4486	44	7	43	+65	4390	28	1	7	-31	4455	59	61	+34	4421±25	1	4421	47	5
NGC 6841	5845	23	3	6	−41	5798	9	1	4	−88	...	...	...	...	...	5828	30	10	−58	5886	5	...	...	1
NGC 0641	...	...	...	...	...	6437	28	4	9	+114	...	...	...	...	...	6438	29	9	+115	6323±17	1	6328	59	7
Averages					+15					+45					-31				+33					

*$< v >$ represents mean measured velocity; σ_v, its standard deviation; N_r, the number of runs in which the galaxy was observed; N_o, the number of observations; N_v, the number of velocities in the NED database; and Δv, the difference between the mean velocity and the respective NED "small error" velocity.

†Velocity on NED with the smallest error.

§Reference to the smallest error NED velocity: (1) *Third Reference Catalogue of Bright Galaxies* (RC3), 1991 (version 3.9); (2) Longhetti et al. (1998); (3) Ramella, Focardi & Geller (1996); (4) Kaldare et al. (2003): (5) Alonso et al. (2003).

TABLE 5
AQUARIUS GALAXY CATALOG

Gal Nr. (1)	Coordinates (J2000.0) α (2)	δ (3)	b_J mag. (4)	R mag. (5)	Cluster name (6)	cz (kms^{-1}) (7)	Error (kms^{-1}) (8)	Code* (9)	Run† (10)
1	$22^h57^m53.61^s$	-21°46′57.6″	18.44	···	A2509B	23915	55	x,A, 6.21	21
2	22 57 56.77	-21 50 01.9	18.09	···	A2509B	25503	56	c,A, 2.89	21
3	22 57 57.54	-21 46 37.9	19.12	···	A2509B	23762	70	e,A, 0.00	21
4	22 58 02.21	-21 53 58.2	18.65	···	A2509B	24007	71	c,A, 4.00	12
5	22 58 02.58	-21 53 51.1	18.62	···	A2509C	40169	19	x,A,14.59	12
6	22 58 02.96	-21 54 01.4	19.62	···	A2509C	40132	26	x,A,10.44	12
7	22 58 03.09	-21 53 45.1	19.80	···	A2509C	40253	56	c,B, 4.18	12
8	22 58 05.22	-21 54 29.5	19.55	···	A2509A	69163	34	x,A, 8.00	12
9	22 58 06.56	-21 54 45.6	19.36	···	A2509A	69774	31	x,A,10.78	12
10	22 58 07.41	-21 48 34.1	18.51	···	A2509B	23640	129	c,B, 2.39	21
11	22 58 08.06	-21 55 02.7	···	···	···	63541	77	e,B, 2.46	12
12	22 58 15.34	-21 56 19.6	···	···	A2509B	23787	63	c,A, 3.31	21
13	22 58 16.57	-23 33 44.9	18.48	···	Aqr005	35160	34	x,A, 9.72	22
14	22 58 20.84	-23 33 38.5	19.24	···	Aqr005	35449	38	x,A, 8.57	22
15	22 58 21.16	-23 36 47.6	17.83	···	Aqr005	34775	39	c,A, 7.00	22
16	22 58 21.34	-21 52 48.8	19.81	···	···	55460	63	x,A, 4.23	21
17	22 58 26.71	-23 37 57.4	18.82	···	Aqr005	34847	44	x,A, 7.65	22
18	22 58 27.06	-21 54 18.2	18.85	···	A2509C	40372	57	c,A, 3.98	21
19	22 58 30.50	-23 39 09.4	18.03	···	Aqr005	35541	43	c,A, 6.47	22
20	22 58 30.62	-23 42 33.2	18.72	···	Aqr005	35100	33	x,A,11.31	22

*Codes are for: type of spectrum (x = cross-correlation, e = emission lines, c = combined absorption and emission lines); quality flag (A,B or C); and "R" parameter.

†Refers to Table 1.

NOTE.—The complete version of this table is in the electronic edition of the journal. The printed edition contains only a sample.

TABLE 6
CLUSTER DATA

AqrCC	Other	Coordinates (J2000.0)			Observed Galaxies				v_r	σ_r
	Name	α	δ	Center*	N_{here}	N_{lit}	Ref.†	N_{gal}	(km s^{-1})	(km s^{-1})
(1)	(2)	(3)	(4)	(5)	(6)	(7)	(8)	(9)	(10)	(11)
001	Aqr001-A	$22^h57^m14.6^s$	-24°58′20″	G	...	7	13,16	7	26542^{+64}_{-82}	184^{+83}_{-15}
001	Aqr001-B	22 58 16.7	-25 00 56	G	...	12	16	12	27348^{+50}_{-18}	114^{+43}_{-23}
005	Aqr005	22 58 32.0	-23 37 37	B?	11	7	16	15	35406^{+86}_{-129}	393^{+62}_{-40}
004	A3949	22 58 52.1	-19 57 17	G	7	...	...	7	47358^{+60}_{-210}	207^{+1008}_{-30}
009	A2518-D	23 00 31.9	-24 19 41	G	...	6	16	6	35143^{+90}_{-292}	383^{+139}_{-67}
009	A2518-C	23 00 44.7	-24 06 22	G	...	7	16	7	32953^{+74}_{-3}	57^{+85}_{-37}
009	A2518	23 00 47.0	-24 09 02	B2	6	15	3,16	17	40471^{+126}_{-149}	547^{+158}_{-90}
009	A2518-B	23 00 57.8	-24 12 08	G	4	5	16	7	27595^{+42}_{-172}	199^{+645}_{-118}
010	A2521	23 02 11.4	-22 01 24	B2	14	5	2,3,5	17	40883^{+463}_{-504}	248^{+289}_{-89}
012	A2526	23 04 34.9	-24 04 11	B2	6	4	16	8	60985^{+69}_{-102}	376^{+332}_{-206}
014	A2527	23 05 20.6	-25 20 19	B2	8	4	16	10	48691^{+207}_{-585}	648^{+153}_{-40}
015	A2528	23 05 36.0	-21 23 03	B	11	1	3	12	28475^{+165}_{-197}	458^{+85}_{-44}
016	A2531	23 06 56.0	-21 39 47	B	6	1	3	7	51873^{+343}_{-198}	560^{+236}_{-59}
017	A2534	23 07 41.5	-22 42 39	B	15	1	3	16	60348^{+328}_{-238}	126^{+479}_{-263}
019	Aqr019-C	23 07 42.4	-25 27 12	G	...	8	16	8	34635^{+339}_{-242}	571^{+175}_{-30}
018	A2536	23 07 46.7	-22 27 31	B	7	1	3	6	59811^{+1143}_{-511}	981^{+206}_{-18}
018	A2536-B	23 07 49.9	-22 29 09	G	9	...	...	8	52575^{+132}_{-181}	353^{+150}_{-74}
019	Aqr019-A	23 08 03.1	-25 41 01	G	...	9	16	9	30860^{+45}_{-110}	313^{+365}_{-170}
020	A2538-2	23 08 28.5	-19 51 20	G	...	23	3,4,9	23	25512^{+91}_{-77}	374^{+74}_{-57}
020	A2538-1	23 08 34.1	-19 52 34	B2	...	21	4,9	21	24099^{+136}_{-137}	465^{+78}_{-55}
019	Aqr019-B	23 08 42.3	-25 30 47	G	...	6	16	6	33017^{+94}_{-181}	274^{+135}_{-55}
022	Aqr022	23 09 03.6	-20 45 15	G	5	1	15	6	24739^{+69}_{-38}	152^{+61}_{-34}
023	A2540	23 09 25.1	-22 10 19	B	8	1	3	9	38875^{+21}_{-16}	38^{+555}_{-12}
024	Aqr024	23 09 54.5	-21 31 30	B	7	...	...	7	33250^{+275}_{-280}	600^{+210}_{-68}
026	A2542	23 10 06.2	-24 29 09	B2	4	6	16	6	50560^{+287}_{-8}	454^{+234}_{-439}
027	Aqr027-C	23 10 06.9	-24 44 19	G	1	6	16	6	36060^{+233}_{-445}	715^{+238}_{-84}
025	A2541	23 10 07.2	-22 59 05	B2	17	2	8	17	34032^{+243}_{-284}	991^{+138}_{-87}
027	Aqr027-B	23 10 13.1	-24 46 35	G	2	9	16	10	32625^{+526}_{-375}	785^{+188}_{-69}
028	A2546	23 10 38.7	-22 38 54	B2	22	1	3	22	33903^{+223}_{-177}	784^{+164}_{-98}
027	Aqr027	23 10 39.9	-24 45 13	B2	5	3	16	6	59786^{+195}_{-252}	465^{+110}_{-46}
029	A2547	23 10 46.7	-21 08 07	B2	12	5	3,12,15	15	45483^{+409}_{-476}	80^{+272}_{-136}
031	A2548	23 11 15.8	-20 25 05	B	6	4	3,15	9	33105^{+81}_{-46}	180^{+73}_{-15}
033	A2550	23 11 35.8	-21 44 47	B	5	2	3,15	6	36752^{+321}_{-329}	517^{+230}_{-22}
035	A2554	23 12 19.9	-21 30 10	B	4	31	3,4,15	32	33243^{+139}_{-166}	868^{+129}_{-68}
036	A2553	23 12 24.8	-24 57 12	B2	...	13	10,16	13	44081^{+191}_{-198}	686^{+161}_{-76}
037	A2555	23 12 51.3	-22 15 27	B?	9	2	15	11	33236^{+25}_{-85}	238^{+84}_{-72}
038	A2556	23 13 01.5	-21 38 04	B	5	8	1,3,4,15	10	26109^{+75}_{-260}	352^{+355}_{-112}
039	S1099	23 13 10.9	-23 09 29	B2	12	...	...	12	33258^{+373}_{-227}	732^{+238}_{-98}
040	Aqr040	23 14 30.8	-23 22 24	B2	6	1	16	7	27274^{+53}_{-42}	122^{+47}_{-20}
041	A2565-A	23 15 52.0	-21 08 30	G	12	...	...	12	24727^{+69}_{-144}	359^{+483}_{-43}
041	A2565-B	23 15 54.9	-21 08 18	G	10	1	3	10	38365^{+86}_{-169}	325^{+76}_{-51}
044	A2566	23 16 05.0	-20 27 48	B	10	2	3,9	11	24642^{+159}_{-439}	856^{+179}_{-154}
042	A3985-2	23 16 12.1	-23 22 55	G	8	2	16	10	33940^{+64}_{-74}	181^{+233}_{-34}
042	A3985-1	23 16 15.1	-23 23 36	B	10	5	16	12	31855^{+189}_{-139}	482^{+115}_{-63}
045	Aqr045-A	23 16 20.9	-25 00 29	G	...	9	16	9	15436^{+21}_{-356}	329^{+104}_{-41}
045	Aqr045-B	23 16 32.1	-24 57 14	G	...	7	16	7	33000^{+581}_{-235}	513^{+190}_{-58}
046	A2568	23 17 11.8	-22 14 23	B?	5	1	3	6	41875^{+102}_{-232}	327^{+280}_{-155}
047	ED275	23 17 33.7	-25 20 30	B2	6	9	16	12	43329^{+241}_{-293}	670^{+192}_{-60}

TABLE 6—*Continued*

AqrCC	Other	Coordinates (J2000.0)			Observed Galaxies				v_r	σ_r
	Name	α	δ	Center*	N_{here}	N_{lit}	Ref.†	N_{gal}	(km s^{-1})	(km s^{-1})
(1)	(2)	(3)	(4)	(5)	(6)	(7)	(8)	(9)	(10)	(11)
051	A2576	23 19 43.9	-22 27 52	B?	...	10	7	10	56253^{+453}_{-458}	750^{+193}_{-65}
052	S1113	23 20 01.8	-24 08 46	B?	9	10	16	14	44005^{+118}_{-98}	367^{+53}_{-47}
055	A2577	23 20 46.7	-22 59 30	B	6	1	10	7	37363^{+61}_{-278}	176^{+92}_{-9}
057	A2579	23 21 15.6	-21 35 04	B	4	6	10,15	10	33409^{+104}_{-143}	394^{+92}_{-46}
061	A2580	23 21 26.3	-23 12 26	B	19	...	...	17	26687^{+173}_{-164}	661^{+130}_{-82}
059	A3997	23 21 33.7	-24 08 52	B3	8	5	16	11	44280^{+133}_{-90}	391^{+455}_{-166}
063	A2583	23 22 14.7	-20 26 08	B?	8	...	...	8	34388^{+237}_{-293}	659^{+264}_{-104}
065	A2586	23 23 24.3	-20 22 35	B	11	...	...	11	43420^{+316}_{-77}	828^{+274}_{-261}
066	A2587	23 23 32.4	-22 25 21	B	6	...	...	6	64750^{+807}_{-131}	673^{+287}_{-101}
067	ED291	23 24 13.2	-22 31 12	G	15	1	15	15	36690^{+94}_{-127}	378^{+88}_{-43}
070	A2596	23 25 05.6	-23 23 49	B2	21	10	13,15,16	27	26719^{+113}_{-117}	496^{+79}_{-36}
069	A2595	23 25 06.2	-20 32 37	B?	5	...	...	5	54091^{+199}_{-561}	545^{+173}_{-21}
073	APM895/894	23 26 14.1	-24 06 30	B	16	36	11,14,15,16	35	33463^{+67}_{-102}	549^{+109}_{-72}
075	A2600	23 26 31.9	-22 25 47	G	6	3	15	9	36268^{+344}_{-164}	570^{+410}_{-125}
074	A2599-B	23 26 38.1	-23 46 04	B	9	9	14,15,16	13	37841^{+109}_{-226}	585^{+344}_{-111}
074	A2599-A	23 26 54.5	-23 51 46	G	9	26	6,8,14,15,16	22	26943^{+128}_{-86}	456^{+105}_{-63}
076	A2601	23 27 01.8	-24 30 04	G	4	4	15,16	7	63552^{+72}_{-307}	635^{+597}_{-219}
075	A2600-B	23 27 11.2	-22 18 55	G	2	7	15	9	18305^{+261}_{-167}	363^{+91}_{-84}
078	ED300-B	23 27 45.4	-25 05 42	G	1	11	16	11	26436^{+170}_{-521}	449^{+139}_{-68}
077	A2603	23 27 56.8	-25 22 37	B	7	3	...	6	63218^{+110}_{-115}	396^{+174}_{-144}
078	ED300	23 28 16.2	-24 56 43	B	12	12	16	18	33480^{+173}_{-143}	585^{+94}_{-41}
081	A2605-A	23 28 48.9	-23 22 22	B2	11	1	15	10	33589^{+222}_{-222}	545^{+154}_{-58}
081	A2605-B	23 29 05.9	-23 25 08	B	6	...	...	6	26621^{+166}_{-170}	266^{+108}_{-22}
091	A4014	23 32 25.7	-25 28 50	B2	11	16	16	22	33840^{+57}_{-46}	261^{+132}_{-37}
099	A2628	23 37 01.4	-24 10 58	G	...	9	7	9	55468^{+217}_{-448}	810^{+247}_{-121}
101	A2629	23 37 47.2	-22 54 42	B?	7	...	...	7	62038^{+405}_{-470}	986^{+327}_{-68}

*Type of projected center: (B#) position of the brightest cluster galaxy (# is the number of giant ellipticals considered as BCGs of the cluster, ? means BCG is not surely defined); (G) geometric mean of the positions of galaxies confirmed as cluster members.

†References of the galaxy velocities from the literature: (1) Kowalski, Ulmer & Cruddace (1983); (2) Schneider, Gunn & Hoessel (1983); (3) Ciardullo, Ford & Harms (1985); (4) Colless & Hewett (1987); (5) Valentijn & Casertano (1988); (6) Dalton et al. (1994); (7) Batuski et al. (1995); (8) Collins et al. (1995); (9) Owen, Ledlow & Keel (1995); (10) Quintana & Ramírez (1995); (11) Loveday (1996); (12) Kapahi et al. (1998); (13) Ratcliffe et al. (1998); (14) Alonso et al. (1999); (15) Batuski et al. (1999); (16) Colless et al. (2001).